THE USE OF MAGNETIC MEASUREMENTS FOR LHC OPERATION

Luca Bottura, CERN, Geneva, Switzerland
Nicholas J. Sammut, CERN, Geneva, Switzerland; University of Malta, Malta

Abstract

An effective accelerator control system can function only when the errors are known to the desired accuracy. Direct diagnostics on the beam is the ideal way of measuring the field errors. However, as described in [1] a system solely based on beam feed-back may be too demanding. Hence, to compensate for the magnet field errors obtained from magnet production and installation, the LHC control system requires an accurate forecast of the magnetic field and the multipole field errors in the accelerator. In this paper we describe how to use warm and cold magnetic measurement data to provide this forecast.

INFORMATION AVAILABLE FROM MAGNETIC MEASUREMENTS ON DAY 1

In order to steer the magnet production and monitor that the field quality is within the required specifications, the LHC quality assurance plan foresees the testing at warm of:

- All the MB, MQ, MQM and MQYs so as to obtain their main field integral strength as well as their higher order geometric harmonics;
- All the MBX, MBRx and MQXx;
- All the MQTL (presently done at CERN);
- Most superconducting lattice correctors and spool pieces (at present the data for 90 % of the produced magnets is available);
- All warm MQW;
- A sample (of about 5 to 10) of other warm insertion magnets (MBXW,..) measured at the manufacturer before delivery.

Standard cold magnetic measurements are currently performed in the cold test benches SM18 and in the vertical cryostats of Block-4. The aim of these cold tests is to obtain a good warm-cold correlation and to enable accurate magnetic field modeling of the LHC during the entire machine cycle. At the present rate, cold measurements are performed on:

- 20% of the MB and 20% of the MQ in standard conditions (i.e. load line and LHC cycle);
- 12 special MB tests to study powering history effect on the decay;
- 12 special MB tests to establish the details of the snap-back waveform;
- A sample of the MQM and MQY (typically 10% in SM-18 and 30% in Block 4);
- 75% of the MBX, MBRx;
- 100% of the MQXx (Q1, Q2, Q3);
- few MQTL (2 cold tests have been performed to date) [2];
- A limited sample of lattice correctors and spool pieces (about 120 tests have been performed to date, while a plan for the over 7000 magnets series is still not completely defined [2]).

An example of the information obtained from the tests of an LHC dipole can be found in Fig 1, reporting the sextupole field as from the data taken at warm in industry, and at cold during a simulated LHC cycle. As described in section 2, a breakdown into different components, identified in the plot, is used to accurately model the data.

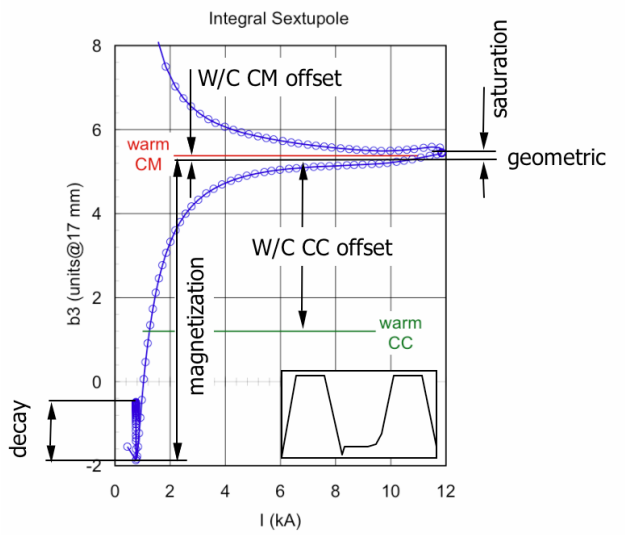

Figure 1: Integral sextupole of typical dipole magnet. The red line is the warm cold mass value, the green line is the warm collared coil value and the black horizontal line is the geometric value.

Presently, the warm and cold magnetic data is stored in three different Oracle databases containing separate entries for:

- Warm data;
- Cold Data (Injection and Flat-Top);
- Warm-Cold Offsets (Injection and Flat-Top);
- Components in cold conditions (geometric, persistent currents, decay, snap-back, saturation).

At the current rate, by the end of 2006, 3.5 million measurements and 35GB of accumulated data will be available in the databases. The plan is to use this data to:

- Set injection values;
- Generate ramps;

- Forecast the corrections of the field errors in MB and IR magnets.

The principle is to define modelling functions for the current and time behaviour of each field error component, and to scale the modelling functions by the value of the measured component which is stored in the database or can be deduced from values stored in the data base (e.g. an extrapolation from warm conditions). This will be done on a magnet *family* basis [3], [4], as described later, where with *family* we intend a group of magnets powered in series, for which the integrated transfer function and integral harmonics information is needed (e.g. the set of 154 dipoles in a sector).

THE FIELD MODEL

One of the key elements of the system that will deliver a forecast of the magnetic field in the LHC is the *field model*. The model is a decomposition of the field errors and their deviations from the reference design values based on a separation of the contributing effects.

In the following we indicate with $\mathbf{C}_n$ the complex harmonic of order n in the complex series expansion of the 2-D magnetic field **B** in the magnet aperture:

$$\mathbf{B}(x,y) = B_y + iB_x = \sum_{n=1}^{\infty} \mathbf{C}_n \left(\frac{\mathbf{z}}{R_{ref}}\right)^{n-1} = \sum_{n=1}^{\infty} (B_n + iA_n)\left(\frac{x+iy}{R_{ref}}\right)^{n-1} \quad (1)$$

where **z** is the coordinate in the complex plane and R_{ref} is the reference radius. The coefficients $\mathbf{C}_n$ have dimensions of [T @ R_{ref}]. Taking the index m as the order of the main field (with m = 1 for dipole), the index n stands for the higher order field harmonics. The index n is therefore such that

$$n \geq m + 1 \quad (2).$$

The main field is indicated as B_m (in T at the reference radius R_{ref}=17mm). The non-normalized harmonic coefficients $\boldsymbol{C}_n$ are assumed to be given in the reference frame aligned with the main field direction. They can be decomposed in their real part B_n (the normal harmonics) and imaginary part A_n (the skew harmonics), and, because we take the main field to be purely normal, we have by definition A_m = 0. For convenience we use also normalized harmonic coefficients, indicated as $\boldsymbol{c}_n$ and defined as:

$$\mathbf{c}_n = b_n + ia_n = 10^4 \frac{\mathbf{C}_n}{B_m} \quad (3)$$

expressed in [units @ R_{ref}], and also decomposed in their real part b_n (the normal harmonics) and imaginary part a_n (the skew harmonics). Finally, the main field transfer function (*TF*) is defined as the ratio of field generated and operating current:

$$TF = \frac{B_m}{I} \quad (4)$$

which is expressed in units of [T @R_{ref} / A].

The field model is the relation:

$$\mathbf{C}_n = \mathbf{C}_n\left(t, I, \frac{dI}{dt}, T, I(-t)\right) \quad (5)$$

where we express the fact that the harmonic $\mathbf{C}_n$ depends on time (t), magnet operating current (I), magnet ramp-rate (dI/dt), magnet temperature (T) and magnet powering history I(-t). To give an explicit form of the field model, we decompose the field errors in the following components:

1) DC Components (steady state, reproducible from cycle to cycle, depend on current, but not on time)

a. *Residual Magnetization Contribution* ($\mathbf{C}_n^{residual}$) of magnetic parts in the cold mass, mostly in the iron surrounding the coils, visible at low current, e.g. during warm measurements;
b. *Geometric Contribution* ($\mathbf{C}_n^{geometric}$): deviation between the conductor placement in the real coil winding and the ideal distribution of current (i.e. producing the exact, desired multipolar field). This contribution is present at all field levels and is proportional to the operating current;
c. *Displacement Contribution* ($\mathbf{C}_n^{deformation}$): displacements of the cables in the coil cross section. Cable movements can take place, for instance, during cool-down and powering at high field as a consequence of the changes in the force and stress distribution;
d. *DC Magnetization Contribution* ($\mathbf{C}_n^{MDC}$): persistent currents in the superconducting filaments. This contribution is important at low operating field (e.g. injection in the main dipoles), where the superconductor magnetization is highest;
e. *Saturation Contribution* ($\mathbf{C}_n^{saturation}$): due to changes of the magnetic permeability in the iron yoke surrounding the coils. This contribution is important at high field, mainly on the main field component.

2) AC Short Term Effects (transient, reproducible, depends on current and time)

a. *Coupling currents* ($\mathbf{C}_n^{MAC}$): due to interfilamentary currents within the strand and interstrand currents within the cable. This contribution is only present during changes in the operating field, e.g. during energy ramp, is reproducible, depends on current and time.

3) AC Long Term Effects (transient, non reproducible, depends on current, time and powering history)

a. *Decay* ($\mathbf{C}_n^{decay}$)*:* effect due to cable internal field changes and, possibly, flux creep in the filaments magnetization, important during injection and in general at all current plateaus at low field;

b. *Snapback* ($\mathbf{C}_n^{snap-back}$)*:* rapid re-establishment of the magnetization after its decay during a constant current plateau, important at the beginning of the acceleration ramp.

The field model will provide the desired field component dependency $\mathbf{C}_n^{component}\left(t, I, dI/dt, T, I(-t)\right)$. As a general rule, superconducting magnets (and especially dipoles and quadrupoles) are designed to achieve relative field errors of 0.1 % or better. For this reason we can safely assume that all deviations from linearity are small perturbations of the ideal field, and that they can be added linearly to obtain the total field in the magnet. Hence, under this assumption, the field model can be given by the sum of the contributions:

$$\mathbf{C}_n = \mathbf{C}_n^{DC} + \mathbf{C}_n^{ACS} + \mathbf{C}_n^{ACL} \tag{6}$$

where $\mathbf{C}_n^{DC}$ is the DC, steady state error, $\mathbf{C}_n^{ACS}$ is the AC short term error and $\mathbf{C}_n^{ACL}$ is the AC long term error respectively defined as:

$$\mathbf{C}_n^{DC} = \mathbf{C}_n^{residual} + \mathbf{C}_n^{geometric} + \\ + \mathbf{C}_n^{deformation} + \mathbf{C}_n^{MDC} + \mathbf{C}_n^{saturation} \tag{7}$$

$$\mathbf{C}_n^{ACS} = \mathbf{C}_n^{MAC} \tag{8}$$

$$\mathbf{C}_n^{ACL} = \mathbf{C}_n^{decay} + \mathbf{C}_n^{snap-back} \tag{9}.$$

The order of magnitude, and hence the importance of the different components identified here, is quite different. Figure 2 gives an ordering based on the order of magnitude, the uncertainty and the variability from magnet to magnet and from cycle to cycle. The components at the top of the list are those that are expected to be most relevant for setting and correction, while those at the bottom of the list can be neglected.

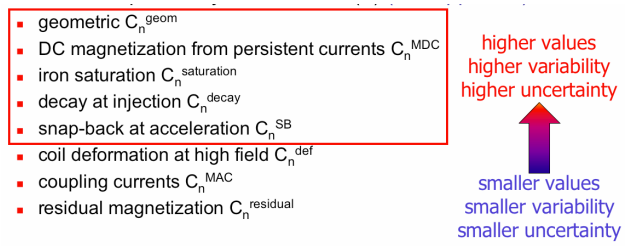

Figure 2: General decomposition of error sources listed in order of importance.

In the following sections we give analytical formulae, suitable to describe the various dependencies, with a limited set of free parameters.

Geometric Contributions

The geometric contributions to the field and field errors is proportional to the excitation current in the magnet. Hence the geometric contribution may be written as:

$$B_m^{geometric} = \gamma_m I \tag{10}$$

where I is the excitation current in the magnet. The geometric coefficient in the above definition includes the linear contribution from the iron yoke thus ignoring the saturation and the residual magnetization. For the transfer function:

$$TF^{geometric} = \gamma_m \tag{11}$$

and for the normalized harmonics:

$$\mathbf{c}_n^{geometric} = \gamma_n \tag{12}$$

The geometric coefficient in its definition above also includes the linear contribution from the iron yoke (i.e. ignoring the saturation and permanent magnetization). This is the only component of the model that can be obtained through extrapolation from warm measurements.

DC Magnetization Contributions

When the background field is varied during the field ramp, the superconducting filaments in a strand become magnetized. The magnetization M is generated by persistent currents trapped in the filaments. Hence, in the first approximation, the magnetization is proportional to the critical current density J_c and the filament diameter D [5]:

$$M \propto J_c D \tag{13}.$$

The critical current density changes with field according to a law of the type [6]:

$$J_c \propto \frac{1}{B}\left(\frac{B}{B_c}\right)^{\alpha}\left(1-\frac{B}{B_c}\right)^{\beta} \qquad (14)$$

where B is the background field, B_c is the critical field of the material, α and β are pinning exponents that are typically in the range $\alpha = 0.5$ and $\beta = 1$ for the NbTi alloy used in the LHC cables [7].

M is essentially stationary in time (DC) and is hysteretic since the persistent currents have exceedingly long time constants. Hence the DC magnetization is visible as a hysteretic contribution to the field and field errors that depends on the strength of the magnetization as well as on the geometric distribution of the magnetization vectors in the winding cross section. Smaller magnetization amplitudes in the high-field regions and larger magnetization in the low-field regions are the result of the presence of large field gradients in the coil. In particular, this is important at injection where the magnitude and variation of M is the largest.

To provide a scaling for the field generated by the DC magnetization it is assumed that this contribution scales as the J_c in Eq. (14). Current is substituted for field giving:

$$B_m^{MDC} = \mu_m \frac{I_{inj}}{I}\left(\frac{I}{I_{inj}}\right)^{\alpha}\left(\frac{I_c - I}{I_c - I_{inj}}\right)^{\beta} \qquad (15)$$

where the injection current I_{inj} is introduced as a reference point so that the product of the three terms in I is equal to the one at I_{inj}, and the value of μ_m can be interpreted as the value of the contribution of the DC magnetization to the total field measured at injection, and presently stored in the database. By writing Eq. (14) the assumption that the complex convolution of the distribution of magnetization vectors can be condensed in the fitting exponents α and β is made. The contribution to the transfer function is:

$$TF^{MDC} = \mu_m \frac{I_{inj}}{I^2}\left(\frac{I}{I_{inj}}\right)^{\alpha}\left(\frac{I_c - I}{I_c - I_{inj}}\right)^{\beta} \qquad (16)$$

and the normalised harmonics originated by the DC magnetization are:

$$\mathbf{c}_n^{MDC} = \mu_n \left(\frac{I_{inj}}{I}\right)^{2-\alpha}\left(\frac{I_c - I}{I_c - I_{inj}}\right)^{\beta} \qquad (17)$$

which has a different form from Eq. (14) because of the renormalization to make μ_n the measured DC magnetization harmonic at injection.

For a monotonous ramp (ramp-up or ramp-down), the Eqs. (15), (16) and (17) hold when the filaments in the coil are in a fully penetrated state, i.e. after the crossing of the hysteresis cycle (penetration phase). The expressions are the same for different ramp directions, but the coefficients μ_m and μ_n for an upwards ramp have opposite sign (and approximately same value) to those that best fit a downwards ramp.

Iron Saturation Contribution

The iron saturation contributions to the main field and field errors depend mostly on the iron yoke configuration and on the B-H characteristics of the iron structure. The iron yoke saturation appears as a non-linearity of the field and the field errors with respect to the operating current. This deviation is especially visible at high field levels, when the extent of saturation becomes significant.

It is not easy to establish an *a priori* fit which can take both effects into account by simple parameterization of the magnet cross section. Therefore the choice is to fit the saturation contribution as a sum of rounded step functions. In practice a function that can be used with good accuracy is:

$$\begin{aligned}&\Sigma\left(I, I_1^{\sigma}, \Delta I_1^{\sigma}, I_2^{\sigma}, \Delta I_2^{\sigma}, a^{\sigma}\right)\\ &= \left[a^{\sigma} S\left(I, I_1^{\sigma}, \Delta I_1^{\sigma}\right) + \left(1-a^{\sigma}\right) S\left(I, I_2^{\sigma}, \Delta I_2^{\sigma}\right)\right]\end{aligned} \qquad (18)$$

where S^{σ} is a normalized, smooth step function that is adapted to describe the change in field associated with saturation:

$$S\left(I, I^{\sigma}, \Delta I^{\sigma}\right) = \frac{1}{\pi}\left[\arctan\left(\frac{I - I^{\sigma}}{\Delta I^{\sigma}}\right) + \frac{\pi}{2}\right] \qquad (19).$$

Figure 3 shows the normalized function.

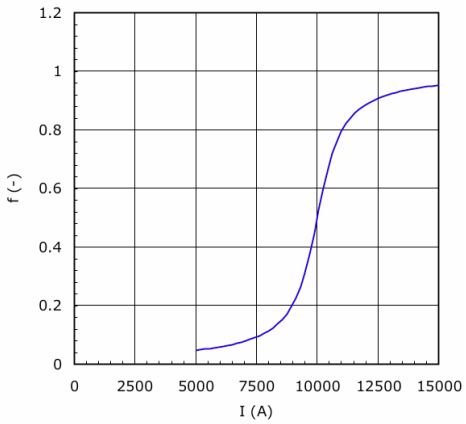

Figure 3. The smooth step function used to describe the change in field due to saturation.

For the main field component:

$$B_m^{saturation} = \sigma_m \, I \frac{\Sigma\left(I, I_1^\sigma, \Delta I_1^\sigma, I_2^\sigma, \Delta I_2^\sigma, a^\sigma\right)}{\Sigma\left(I_{nom}, I_1^\sigma, \Delta I_1^\sigma, I_2^\sigma, \Delta I_2^\sigma, a^\sigma\right)} \quad (20).$$

The transfer function is correspondingly:

$$TF^{saturation} = \sigma_m \frac{\Sigma\left(I, I_1^\sigma, \Delta I_1^\sigma, I_2^\sigma, \Delta I_2^\sigma, a^\sigma\right)}{\Sigma\left(I_{nom}, I_1^\sigma, \Delta I_1^\sigma, I_2^\sigma, \Delta I_2^\sigma, a^\sigma\right)} \quad (21)$$

and the harmonic coefficients are:

$$\mathbf{c}_n^{saturation} = \boldsymbol{\sigma}_n \frac{\Sigma\left(I, I_1^\sigma, \Delta I_1^\sigma, I_2^\sigma, \Delta I_2^\sigma, a^\sigma\right)}{\Sigma\left(I_{nom}, I_1^\sigma, \Delta I_1^\sigma, I_2^\sigma, \Delta I_2^\sigma, a^\sigma\right)} \quad (22).$$

Decay

It has been shown by [8] that the decay of harmonics at constant current is driven by field changes on the strands caused by current redistribution in the superconducting cables. The amplitude of the current distribution process can be modeled by a diffusion equation, whose most general solution is a series of harmonics in space modulated by an exponential dependence in time. The decay phenomenon is quite complex: the current redistribution causes a change of the local field in the coil by few mT, which in turn changes the persistent currents distribution and the DC magnetization of the filaments by adding an arbitrary component to the initial magnetization state. This results in a net decrease of the average DC magnetization of the cables and an overall decrease of its contribution to the total field. Neglecting all non-linearities, we make here the simplifying assumption that the dynamics of the field follows that of the current diffusion. The evolution follows the function [9]:

$$\Delta\left(t, t_{inj}, \tau, a^\Delta\right) = \left[a^\Delta \left(1 - e^{-\frac{t - t_{inj}}{\tau}}\right) + \left(1 - a^\Delta\right)\left(1 - e^{-\frac{t - t_{inj}}{9\tau}}\right)\right] \quad (23)$$

where t is the time, t_{inj} is the time at injection, τ is the time constant. a^Δ gives the normalized weight of the fast component of the decay and its complement to one, $1-a^\Delta$, gives the normalized weight of the slow component. The field decay, using Eq. (23), is given by:

$$B_m^{decay} = \delta_m \frac{\Delta\left(t, t_{inj}, \tau, a^\Delta\right)}{\Delta\left(t_{inj}^{std}, t_{inj}, \tau, a^\Delta\right)} \quad (24)$$

where the parameter δ_m represents the maximum decay, following an infinitely long injection. The contribution to the transfer function is given by:

$$TF^{decay} = \frac{\delta_m}{I} \frac{\Delta\left(t, t_{inj}, \tau, a^\Delta\right)}{\Delta\left(t_{inj}^{std}, t_{inj}, \tau, a^\Delta\right)} \quad (25)$$

and by analogy the contribution to the harmonics is given by:

$$\mathbf{c}_n^{decay} = \boldsymbol{\delta}_n \frac{\Delta\left(t, t_{inj}, \tau, a^\Delta\right)}{\Delta\left(t_{inj}^{std}, t_{inj}, \tau, a^\Delta\right)} \quad (26).$$

The amount of decay depends mostly on the powering history. In practice the powering history can be condensed in a single powering cycle characterized by the current reached at the flat-top I_{FT}, the flat-top duration t_{FT}, the time $t_{preparation}$ elapsed (ramp-down, preparation, ramp to injection) between the end of the flat-top and the injection. The scaling for the decay amplitudes are as follows:

$$\delta_n = \delta_n^{std} \left(\frac{I_{FT}}{I_{FT}^{std}}\right) \left(\frac{A - Be^{-\frac{t_{FT}}{\tau}}}{A - Be^{-\frac{t_{FT}^{std}}{\tau}}}\right) \left(\frac{C + De^{-\frac{t_{preparation}}{\tau}}}{C + De^{-\frac{t_{preparation}^{std}}{\tau}}}\right) \quad (27).$$

Snap-back

During snap-back the field *bounces back* to its pre-decay level once the current in the magnet starts to ramp up after a stop, e.g. at injection. Fast sextupole measurements in the LHC and Tevatron main bending dipole magnets have shown that the sextupole snap-back can be described well (within a standard deviation of 0.02 units) by an exponential fitting of the type [9]:

$$b_3^{snap-back}(t) = \Delta b_3 e^{-\frac{I(t) - I_{injection}}{\Delta I}} \quad (28)$$

where $b_3^{snap-back}(t)$ is the sextupole change during the snap-back, $I(t)$ is the instantaneous value of the current, initially at the injection value I_{inj}. The snap-back amplitude Δb_3 and the current change ΔI are the two fitting constants. In addition, the fitting parameters are strongly correlated, and once represented in a scatter plot Δb_3 vs. ΔI they lie on a straight line [9]:

$$\Delta b_3 = \xi_3 \Delta I \quad (29)$$

where ξ_3 is a constant. Based on this observation the snap-back can be modeled by an expression of the type given above so that:

$$B_m^{snap-back} = \Delta b_m I e^{-\frac{I(t) - I_{inj}}{\Delta I}} \quad (30)$$

$$TF^{snap-back} = \Delta b_m e^{-\frac{I(t)-I_{inj}}{\Delta I}} \quad (31)$$

$$\mathbf{c}_n^{snap-back} = \Delta \mathbf{c}_n^{decay} e^{-\frac{I(t)-I_{inj}}{\Delta I}} \quad (32)$$

where the characteristic current change ΔI is given by:

$$\Delta I = \frac{\Delta c_n}{\xi_n} \quad (33).$$

Displacement Contributions

In general contributions due to coil deformation under electromagnetic loads are proportional to the Lorentz forces, and appear as non linear field errors in the field. In the first approximation, in case the constraints do not change during powering these errors are proportional to the square of the current. Unfortunately depending on the real dynamics of the structure, complex situations of establishment or loss of contact may arise. The contacts may be established or not depending on the amount of pre-stress in the structure. In general, the changes in field and field errors can only be obtained in detail using simulation codes that take into account the actual deformation for the specific pre-load case and hence reconstruct the change in the field.

Since the effect of the coil movement has been found to be small it can be approximated by a term proportional to the Lorentz force, i.e.:

$$B_m^{deformation} = \delta_m \left(\frac{I}{I_{nom}} \right)^3 \quad (34)$$

which is normalized so that the coefficient δ_m corresponds to the effect measured at nominal current I_{nom}. For the transfer function:

$$TF^{deformation} = \delta_m \frac{I}{I_{nom}^2} \quad (35)$$

Similarly for the field errors;

$$\mathbf{c}_n^{deformation} = \delta_n \left(\frac{I}{I_{nom}} \right)^2 \quad (36).$$

Coupling Currents Contribution

Eddy currents are induced in loops among the transposed superconducting filaments in the strands, or among the strands in the cables. These currents *couple* the filaments and strands electromagnetically and are often referred to as *coupling* currents. They have time constants in the range of few milliseconds (among filaments in the strands) to few hundreds of milliseconds (among strands in cables). Therefore, for the typical ramp times to be used in the LHC operation, they can be assumed to be fully developed in the *resistive regime*, that is all inductive and shielding effects have already decayed. We also neglect the field dependence of the total resistance of the coupling current loops.

With this assumption, the contribution of coupling currents to main field and field errors is linear with the ramp-rate. We write therefore for the main field component that:

$$B_m^{MAC} = \theta_m \frac{1}{10} \frac{dI}{dt} \quad (37)$$

where the normalization factor is used to refer the contribution to the nominal ramp-rate of the LHC (10 A/s). The contribution to the transfer function is:

$$TF^{MAC} = \theta_m \frac{I_{inj}}{10I} \frac{dI}{dt} \quad (38)$$

while for the normalized harmonics:

$$\mathbf{c}_n^{MAC} = \theta_m \frac{I_{inj}}{10\, I} \frac{dI}{dt} \quad (39).$$

Note that normalization is such that the multiplication constant corresponds to the effect of the coupling currents at injection current and nominal ramp-rate in both cases.

Residual Magnetization Contributions

After powering at nominal current, some components (e.g. the iron yoke) can be permanently magnetized. This is particularly important in warm conditions and small excitations. The contribution to the main field can be written as:

$$B_m^{residual} = \rho_m \quad (40)$$

for the transfer function:

$$TF^{residual} = \frac{\rho_m}{I} \quad (41)$$

and for the field errors:

$$\mathbf{C}_n^{residual} = \rho_n \quad (42).$$

Note that in the above expression, non-normalized harmonics are used because one cannot use the assumption of a dominating main field with respect to the residual field.

EXAMPLES

Although a practical implementation of the field model is not yet available, we are testing the prediction capability of each single part separately to assess the potential. To give a flavour for the use of the field model, we present here two examples of application: the calculation of the current for injection in sector 7-8, and the forecast of the sextupole error along a standard LHC cycle.

Injection setting for sector 7-8

For beam injection it is necessary to determine the current (I) in the MB of a sector to obtain a given integrated field Bdl. As most magnets of sector 7-8 have been allocated [10] and prepared for installation, we can try and produce a forecast of the current to be used for injection test, to be performed late in 2006. The prediction is based on 109 out of 154 magnets, of which 65 have been cold measured and 44 only have warm measurements. The algorithm used is the following:

1) For the magnets missing cold data, we have:
   a) retrieved warm transfer function TF_w^M for each magnet M in the sector
   b) apply the warm-cold scaling f_{TF} and offset $\bullet_{TF}(I)$ to obtain the cold transfer function TF_c^M

$$TF_c^M = f_{TF} TF_w^M + \Delta_{TF} \qquad (43).$$

2) Integrate the transfer function TF_c^M for each magnet M in the sector:

$$TF_c = \sum_M TF_c^M \qquad (44).$$

3) Compute the current by inversion of the (non-linear) $TF_c(I)$:

$$I = \left(TF_c(I)\right)^{-1} Bdl \qquad (45).$$

The warm-cold correlation, as computed in July 2004 on approximately 100 magnets, has a stable offset (at injection $\bullet_{TF}$ =4.0 units, at nominal $\bullet_{TF}$ =-54.2 units). The standard deviation is also acceptable and comparable with the expected measurement accuracy (at injection σ = 5.5 units; at nominal σ = 5.0 units). The result is that the transfer function in the two apertures is:

		Beam 1	Beam 2
TF_{78}	(T m / kA)	10.1175	10.1171

Hence the current in sector 7-8 for an injection at 450GeV from SPS (1189.2 T m) is:

$$I_{78} = 763.25 \text{ A}.$$

Sextupole error forecast

We have performed a second exercise to predict the sextupole field error during an LHC ramp. In this case only the dominating error componets were considered, i.e. the geometric error, the DC magnetization from persistent currents, decay and snap-back and iron saturation. The results are reported in Fig. 4, and show that the modelling can be quite effective. The maximum error is found during the ramp, and is of the order of 0.2 units @ 17 mm (i.e. below 10 units of chromaticity). As a word of caveat, this test was performed for a standard excitation cycle, and does not take into account the variability of decay and snap-back from cycle to cycle, that tends to increase the error.

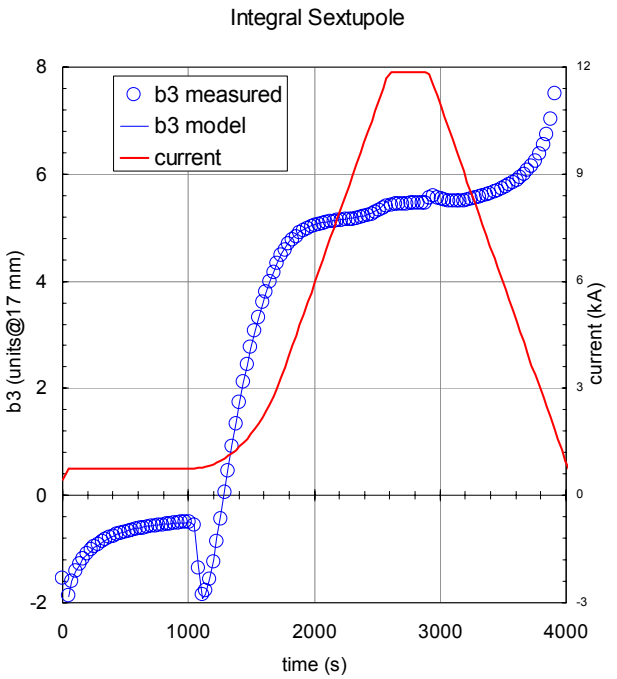

Figure 4: Modelling of the nornal sextupole during a simulated LHC cycle. The maximum error is of the order of 0.2 units @ 17 mm during the ramp.

A SKETCH OF A DESIGN

We have described in some details the elements of the machinery that can provide a forecast of current ramps and corrections. In Fig. 5 we show a starting point for the design of this machinery. At the present status we plan to have a program that contains the laws detailed previously for the interpolation of the field and field errors. By definition, the scaling coefficients for the interpolating functions are the results of the analysis of warm and cold magnetic measurements. These can be retrieved from the databases where they are stored. The query will be made based on the slot position in the tunnel, using the

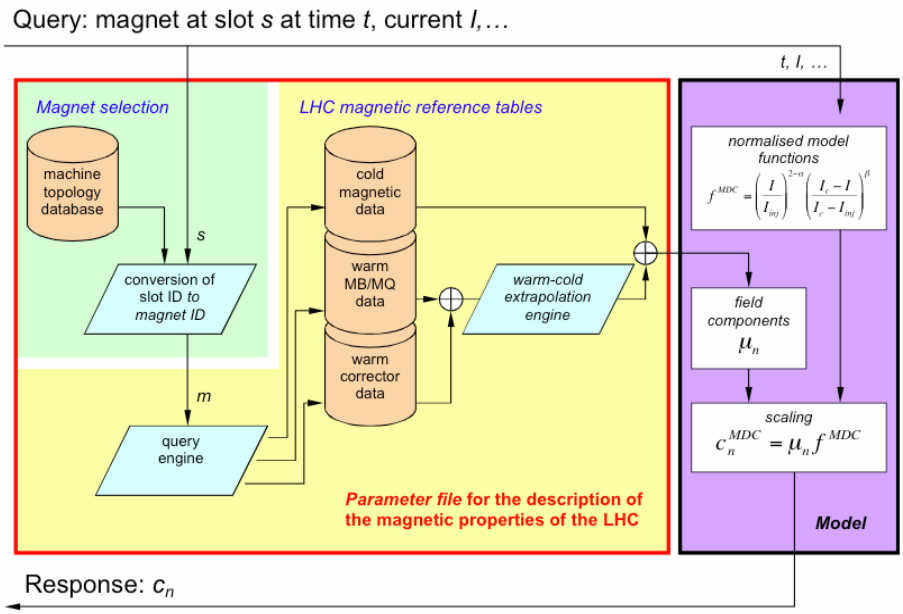

Figure 5: A conceptual design for the "thing", the LHC Magnetic Field Model, showing the relation to information stored in databases and the processing of the request for a field forecast.

installation sequence to make the correspondence between the tunnel slot (relevant for the beam) and the magnet (the index in the magnetic databases).

The databases queries are lengthy and complex, and require time to be exectuted. This would not be acceptable for a real time control algorithm. For this reason the link to databases will be substituted by a data extraction once the machine will be completely allocated (and installed), in a medium size file that will represent the magnetic field properties of the LHC. Detaching from databases will allow for converting the program into the fast tool required for LHC control.

CONCLUSION

From the arguments presented above, one appreciates the fact that warm and cold magnetic measurements can be integrally used for the commissioning and operation of the LHC. The magnet setting and correction forecast is a manageable non-linear problem but requires as from today:

- Extension to magnets other than dipoles;
- Cross-calibration between measurements to decrease the error margins on the settings (like the transfer function for MQ and high order correctors);
- Special measurements to have a sufficient sample for interpolation and extrapolation of field errors (e.g. b3 at injection and ramp) [11];
- Studies to establish a physical description of the magnetic field and the errors to provide a robust model for control (e.g. corrector hysteresis).

The typical prediction error expected for the dipole modelling has been characterized in detail, and is given in Fig. 6 (top). One of the main parameters, the chromaticy, will be uncertain at the 20 to 40 units level. The coefficients of the model are however not frozen, and can be adapted based on the results of beam measurements or special measurement campaigns on spare and left-over magnets, performed on the cryogenic benches used for series tests. This will allow to refine the prediction capability, typically on a time basis of few months, up to a level that we estimate in Tab. 2. In this case the fill-to-fill reproducibility is expected to be as good as 10 units of chromaticity.

	sampling and W/C extrapolation	measurement	magnet stability	powering cycles	commissioning	machine stops	fill-to-fill
b1	4.19	6.81	2.77	1.19	8.55	3.02	1.19
a1	0.85	6.76			6.82		
b2	0.26	0.11	0.05		0.29	0.05	
a2	0.46	0.12	0.25		0.54	0.25	
b3	0.61	0.31	0.27	0.41	0.85	0.49	0.41
a3	0.09	0.04	0.14		0.17	0.14	
b4	0.06	0.05	0.03		0.08	0.03	
a4	0.15	0.05	0.02		0.15	0.02	
b5	0.16	0.06	0.04	0.14	0.22	0.15	0.14

	sampling and W/C extrapolation	measurement	magnet stability	powering cycles	commissioning	machine stops	fill-to-fill
b1	4.19	6.81	2.77	*0.60*	8.49	2.84	0.60
a1	0.85	6.76			6.82		
b2	0.26	0.11	0.05		0.29	0.05	
a2	0.46	0.12	0.25		0.54	0.25	
b3	0.61	0.31	0.27	*0.21*	0.77	0.34	0.21
a3	0.09	0.04	0.14		0.17	0.14	
b4	0.06	0.05	0.03		0.08	0.03	
a4	0.15	0.05	0.02		0.15	0.02	
b5	0.16	0.06	0.04	*0.07*	0.18	0.08	0.07

Figure 6: Expected uncertainty on the prediction of dipole field errors at the beginning of operation (top) and after recalibration through comparison with beam-based measurements or using data from magnetic measurements performed on spare magnets during LHC operation (bottom).

For the time being our focus is on realising a first version of the field model for tracking studies. The design will be kept compatible with the requirements for control (fast operation, real-time response).

REFERENCES

[1] L. Deniau, "The LHC Reference Magnetic System", LHC Project Workshop – Chamonix XIII pgs 190-195, January 2004.

[2] W. Venturini, "Magnetic Behavior of the Correctors: Issues for Machine Operation", Contribution to this workshop.

[3] N. Sammut, L. Bottura, "Classification of LHC Dipoles at Injection", CERN Internal Note, EDMS 501792, 2004-10-01

[4] N. Sammut, L. Bottura, "Classification of LHC Dipoles at Injection: Part 2", CERN Internal Note, EDMS 501792, 2004-12-06

[5] P. Schmüser, "Superconductivity", CAS CERN Accelerator School on Superconductivity in Particle Accelerator, CERN 96-03, May 96

[6] K.-H. Mess, P. Schmüser, S. Wolff, "Superconducting Accelerator Magnets", Ed. World Scientific, Singapore, 1996

[7] L. Bottura, "A Practical Fit for the Critical Surface of NBTI", Proceedings to the International Conference on Magnet Technology, pp 1054-1057, Ponte Vedra Beach USA, 1999

[8] A.P. Verweij, "Electrodynamics of Superconducting Cables in Accelerator Magnets", Ph.D. Thesis, Twente University, The Netherlands, 1995.

[9] L. Bottura, T. Pieloni, N. Sammut, 'Scaling Laws for the Field Quality at Injection in the LHC Dipoles', CERN Project Note 361, 2005-02-21

[10] L. Bottura, 'Installation Strategy: which lessons from sector 7/8?', Contribution to this workshop

[11] L. Bottura, N. Sammut, S. Sanfilippo, 'A Proposal for extended Tests for Dipoles and Quadrupoles Measurements for 2005 and 2006', CERN Internal Memo, EDMS: 566058, 25/01/2005